第 35 卷 第 3 期 原 子 核 物 理 评 论 Vol. 35, No. 3
2018 年 9 月 Nuclear Physics Review Sep., 2018

Article ID: 1007-4627(2018) 03-0257-07

Systematic Study of Proton Radioactivity Based on Two-potential Approach with Folding Potentials

CHEN Jiulong[1], CHENG Junhao[1], DENG Jungang[1], LI Xiaohua[1,2,†]

(*1. School of Nuclear Science and Technology, University of South China, Hengyang 421001, Hunan China;*
2. Key Laboratory of Low Dimensional Quantum Structures and Quantum Control,
Hunan Normal University, Changsha 410081, China)

Abstract: In the present work, we systematically study the half–lives of proton radioactivity for $51 \leqslant Z \leqslant 83$ nuclei within the two–potential approach. The total emitted proton–daughter nucleus interaction potential is composed of the microscopic nuclear potential obtained by single folding the density of the daughter nucleus with the DDM3Y effective interaction, the realistic Coulomb potential obtained by single folding the charge density of the daughter nucleus with the proton–proton Coulomb interaction and the centrifugal potential. We extend our study to predict proton radioactivity half–lives of 16 nuclei in the same region within a factor of 4.11. In addition, the Geiger–Nuttall law for proton radioactivity is researched. The results indicate that the Geiger–Nuttall law can be used to describe the proton radioactivity isotopes with same angular momentum.

Key words: proton radioactivity; two-potential approach; folding potential; Geiger–Nuttall law

CLC number: O571.3 **Document code:** A **DOI:** 10.11804/NuclPhysRev.35.03.257

1 Introduction

Proton radioactivity is an important mode of nuclear decay of far from β−stability nuclei. The proton-rich nuclei lying beyond the proton drip line can spontaneously emit protons because the last proton binding energy of those nuclei are negative. In 1970, Jackson et al. firstly observed the proton emission from the isomeric state of ^{53}Co[1–2]. In 1982, Hofmann et al. and Klepper et al. firstly detected the proton emission from nuclear ground states in ^{151}Lu[3] and ^{147}Tm[4] independently. With the development of experimental facilities and radioactive nuclear beams, there are about 28 proton emitters decaying from their ground states to isomeric or ground states and 20 different nuclei choosing to emit protons from the isomeric states, having been identified between $Z = 51$ and $Z = 83$[5–7]. Moreover, the proton radioactivity can provide some important nuclear structure information of the nuclei lying beyond the proton drip lines such as the coupling between bound and unbound nuclear states, the shell structure[8] and so on. It has become a very interesting topic in both the experimental and theoretical research area.

The proton radioactivity can be processed by the Wentzel-Kramers-Brillouin (WKB) approximation method since this process can be treated as a simple quantum tunneling effect through a potential barrier. There are many methods to investigate the proton radioactivity such as the effective interactions of density-dependent M3Y (DDM3Y)[9–11] and Jeukenne, Lejeune and Mahaux (JLM)[11], the unified fission model[12], the generalized liquid–drop model[13–15], the proton radioactivity within a hybrid method[16] and so on. In 2005, Basu *et al.*[9] used the single–folding model to study the half-life of proton radioactivity, their calculations are in good agreement with the experimental data. Moreover, the proton radioactivity shares the same physical mechanism as α decay. Recently, using the two–potential approach(TPA)[17–18], we have done a series of works on α decay[19–26]. In this work, we extend the TPA to

Received date: 13 May 2018; **Revised date:** 30 Jun. 2018

Foundation item: National Natural Science Foundation of China (11205083, 11505100); Construct Program of the Key Discipline in Hunan Province, Research Foundation of Education Bureau of Hunan Province, China (15A159); Natural Science Foundation of Hunan Province, China (2015JJ3103, 2015JJ2121); Innovation Group of Nuclear and Particle Physics in USC; Shandong Province Natural Science Foundation, China (ZR2015AQ007)

Biography: CHEN Jiulong(1994–), Hubei, Postgraduate, Studying on nuclear physics;

† **Corresponding author:** LI Xiaohua, E-mail: lixiaohuaphysics@126.com.

the study of proton radioactivity half–life, while the total emitted proton–daughter nucleus interaction potential is composed of the microscopic nuclear potential obtained by single folding the density of the daughter nucleus with the DDM3Y effective interaction, the realistic Coulomb potential obtained by single folding the charge density of the daughter nucleus with the proton–proton Coulomb interaction and the centrifugal potential.

This article is organized as follows. In Section 2, the theoretical framework for the calculation of the proton radioactivity half–life is briefly described. The detailed calculations and discussion are presented in Section 3. Finally, a brief summary is given in Section 4.

2 Theoretical framework

The TPA was proposed by Gurvitz *et al.*[18] to deal with decay of a quasistationary state that bridges the bound and scattering states, it has been widely applied to calculate the half-life of decaying nucleus[20–21]. In the TPA framework, the proton radioactivity half–life $T_{1/2}$ is calculated as

$$T_{1/2}=\frac{\hbar\ln 2}{\Gamma}, \tag{1}$$

the proton radioactivity width Γ is given by

$$\Gamma=\frac{\hbar^2 F}{4\mu}P, \tag{2}$$

where $\hbar$ is the reduced Planck constant. $\mu=m_{\rm p}m_{\rm d}/(m_{\rm p}+m_{\rm d})$ is the reduced mass of the decaying nuclear system with $m_{\rm p}$ and $m_{\rm d}$ being the mass of proton and daughter nucleus. P is the barrier penetration probability calculated by the WKB approximation, it can be expressed as

$$P=\exp\left(-2\int_{R_2}^{R_3}k(R){\rm d}R\right), \tag{3}$$

where $k(R)=\sqrt{\frac{2\mu}{\hbar^2}|Q_{\rm p}-V(R)|}$ is the wave number of emitted proton, R is the distance between the proton and the mass center of the daughter nucleus. $Q_{\rm p}$ is the proton radioactivity released energy, $V(R)$ is the total emitted proton–daughter nucleus interaction potential including nuclear potential $V_{\rm N}(R)$, Coulomb potential $V_{\rm C}(R)$ and centrifugal potential $V_l(R)$.

The normalization factor F represents the assault frequency, which is related to the integral of the wave function in the internal potential well, and can be approximated as

$$F\int_{R_1}^{R_2}\frac{1}{2k(R)}{\rm d}R=1, \tag{4}$$

where R_1, R_2, and the above R_3 are the three classical turning points, which satisfy the conditions $V(R_1)=V(R_2)=V(R_3)=Q_{\rm p}$.

In this work, the microscopic nuclear potential $V_{\rm N}(R)$ is obtained by single folding the density of the daughter nucleus with the finite range realistic DDM3Y effective interaction[27–29] as

$$V_{\rm N}(R)=\int\rho(\boldsymbol{r})v(s=|\boldsymbol{R}-\boldsymbol{r}|){\rm d}\boldsymbol{r}, \tag{5}$$

where $s=|\boldsymbol{R}-\boldsymbol{r}|$ is the distance between the emitted proton and the nucleon in the daughter nucleus, $\boldsymbol{R}$ and $\boldsymbol{r}$ are the coordinates of the emitted proton and a nucleon belonging to the daughter nucleus with respect to its center. ρ is the density distribution function of the daughter nucleus. In this work, we choose it as a standard Fermi-form[30] as

$$\rho(r)=\frac{\rho_0}{1+\exp(\frac{r-c}{a})}, \tag{6}$$

where

$$c=r_\rho(1-\pi^2a^2/3r_\rho^2),\ r_\rho=1.13A_{\rm d}^{1/3}\ \text{and}\ a=0.54\ \text{fm}, \tag{7}$$

the value of ρ_0 is determined by integrating the volume integral of the density distribution function being equal to the mass number of the residual daughter nucleus. The touching radial separation $R_{\rm c}$ between the proton and the daughter nucleus, the upper limit of the density integral of nuclear potential, is given by[9] $R_{\rm c}=c_{\rm p}+c_{\rm d}$, where $c_{\rm p}$ and $c_{\rm d}$ are obtained by Eq. (7).

The $v(s)$ is the interaction potential between any such two nucleons, as the density dependence in M3Y interaction (DDM3Y) effective[31–32] interaction given by the following

$$v(s,\rho,E)=t^{\rm M3Y}(s,E)g(\rho,E), \tag{8}$$

where $t^{\rm M3Y}$ is given by the Yukawa form[28] and an exchange term interaction with δ. It can be expressed as

$$t^{\rm M3Y}=7999\frac{\exp(-4s)}{4s}-2134\frac{\exp(-2.5s)}{2.5s}+J_{oo}(E)\delta(s), \tag{9}$$

the single-nucleon exchange term $J_{oo}(E)$ is given by

$$J_{oo}(E)=-276(1-0.005E/A_p)\ (\text{MeV}\cdot\text{fm}^3), \tag{10}$$

where E and $A_{\rm p}$ are the laboratory energy and mass number, respectively. According to Ref. [9], E and $A_{\rm p}$ can be replaced as $E/A_{\rm p}=Q_{\rm p}m/\mu$, with m being the nucleonic mass. The density–dependent part[33] has been taken to be the following

$$g(\rho,E)=C[1-\beta(E)\rho^{2/3}], \tag{11}$$

where C and β are the interaction constants in the single–folding model, their values are taken from Ref. [34], chosen as 2.07 and 1.624 fm^2, respectively.

The realistic Coulomb potential $V_{\rm C}(R)$, obtained by single folding integral of the proton–proton Coulomb interaction with the charge density distributions of daughter nucleus, is expressed as

$$V_{\rm C}(R)=\int\rho'(\boldsymbol{r})\frac{e^2}{|\boldsymbol{R}-\boldsymbol{r}|}{\rm d}\boldsymbol{r}, \tag{12}$$

where the charge density distribution of daughter nucleus $\rho'(r)$ is chosen the same form as Eq. (6). The parameter a=0.54 fm and the parameter ρ'_0 is determined by the constrained condition of charge numbers of residual daughter nucleus $Z_{\rm d}$ as

$$\int\rho'(\boldsymbol{r}){\rm d}\boldsymbol{r}=Z_{\rm d}. \tag{13}$$

Because $l(l+1)\rightarrow(l+\frac{1}{2})^2$ is a necessary correction for one–dimensional problems[35], we adopt the Langer modified centrifugal potential, which can be written as

$$V_l(R)=\frac{\hbar^2(l+\frac{1}{2})^2}{2\mu R^2}, \tag{14}$$

where l is the orbital angular momentum taken away by the emitted proton. The minimum orbital momentum $l_{\rm min}$ taken away by the emitted proton can be obtained by the parity and angular momentum conservation laws.

For a more intuitive displaying the relationship between the total emitted proton–daughter nucleus interaction potential $V(R)$ and the separation R, taking nuclear ^{145}Tm as an example, we plot the variation of $V(R)$ with R in Fig. 1.

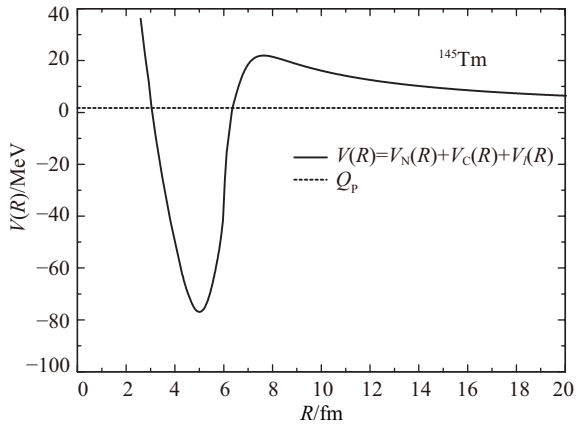

Fig. 1　The variation of the total emitted proton–daughter nucleus interaction potential $V(R)$ with separation R for ^{145}Tm.

3　Results and discussion

In this work, we calculate the half–lives of proton radioactivity for the nuclei from ^{105}Sb to ^{185}Bi^m within the two–potential approach with microscopic nuclear potential and realistic Coulomb potential. The experimental proton radioactivity half–lives, spin and parity are taken from the latest evaluated nuclear properties table NUBASE2016[36] expect for ^{105}Sb, ^{109}I, ^{140}Ho, ^{150}Lu, ^{151}Lu, ^{159}Re$^{\rm m}$, ^{160}Re, ^{164}Ir$^{\rm m}$, which are taken from Ref. [39], the proton radioactivity released energies are taken from the latest evaluated atomic mass table AME2016[37–38]. The detailed results are given in Table 1. In this table, the first two columns present the proton emitter and corresponding proton radioactivity released energy $Q_{\rm p}$, respectively. The following two columns denote the transferred minimum angular momentum $l_{\rm min}$ and the spin–parity transformation taken away by the proton, respectively. R_1, R_2 and R_3 are the three classical turning points obtained by solving the equations $V(R_i)=Q_{\rm p}$ (i=1, 2, 3). The last three columns are the half-lives of the experimental data, the calculated results of the present work and the results of Basu *et al.*, respectively. In this table, we can see that the R_1 are basically the same with the same angular momentum l, and R_1 are obviously different when the angular momentum l are different. It indicates that the effect of orbital momentum l is significant to R_1. For most of the nuclei, the values of R_2 and R_3 are basically in the range of 5 fm to 10 fm and 60 fm to 110 fm, respectively. For the nucleus ^{105}Sb, particularly, the R_3= 148.43 fm is bigger than one of the any other nuclei since its $Q_{\rm p}$ value is smaller than one of these nuclei. In addition, we can clearly see that the calculated values are in good agreement with the experimental data. The standard deviation σ indicating the deviation between the experimental data and calculated ones can be expressed as

$$\sigma=\sqrt{\frac{1}{N}\sum_{i=1}^{N}(\log_{10}T^{\rm calc}_{1/2,i}-\log_{10}T^{\rm expt}_{1/2,i})^2}. \tag{15}$$

In this work, the standard deviation value $\sigma=0.614$ for 41 proton emission nuclei displayed in Table 1. It also shows that the calculations can well reproduce the experimental data. For a more intuitive study, we plot the logarithmic differences between $T^{\rm calc}_{1/2}$ and $T^{\rm expt}_{1/2}$ for those proton emission nuclei in Fig. 2. From this figure, we can clearly see that the values of $\log_{10}T^{\rm calc}_{1/2}/T^{\rm expt}_{1/2}$ are mainly around zero especially for the nuclei from ^{145}Tm to ^{167}Ir^m. For nuclei ^{113}Cs, ^{121}Pr, ^{130}Eu, ^{131}Eu, ^{135}Tb, ^{141}Ho$^{\rm m}$, ^{177}Tl$^{\rm m}$ and ^{185}Bi$^{\rm m}$ there has been a large deviation between calculation and exper-

Table 1 Comparison between the experimental and calculated half–lives of proton decay. The symbol m and n denotes the isomeric state. ′()′ means uncertain spin and / or parity. ′#′ means values estimated from trends in neighboring nuclides with the same Z and N parities.

Nucleus	$Q_{\rm p}$/MeV	$j_{\rm p}^{\pi} \to j_{\rm d}^{\pi}$	$l_{\rm min}$	R_1/fm	R_2/fm	R_3/fm	$\log_{10}T_{1/2}^{\rm expt}$	$\log_{10}T_{1/2}^{\rm calc}$	$\log_{10}T_{1/2}^{\rm SFM}$
^{105}Sb	0.491	$5/2^+ \to 0^+$	2	1.49	6.07	148.43	2.086	1.693	1.97
^{109}I	0.821	$(3/2^+) \to 0^+$	2	1.50	6.15	92.92	−3.897	−4.504	
^{112}Cs	0.821	$1^+\# \to 5/2^+\#$	2	1.51	6.19	96.35	−3.310	−3.763	
^{113}Cs	0.972	$(3/2^+) \to 0^+$	2	1.51	6.22	81.64	−4.752	−5.843	
^{121}Pr	0.891	$(3/2^+) \to 0^+$	2	1.53	6.33	95.28	−1.921	−3.420	
^{130}Eu	1.031	$(1^+) \to (3/2^+, 1/2^+)$	0	0.31	6.58	86.66	−3.000	−4.085	
^{131}Eu	0.951	$3/2^+ \to 0^+$	2	1.85	6.48	95.31	−1.703	−3.019	
^{135}Tb	1.181	$(7/2^-) \to 0^+$	3	2.34	6.45	80.71	−2.996	−4.352	
^{140}Ho	1.092	$6^-, 0^+, 8^+ \to (7/2^+)$	3	2.36	6.52	89.65	−2.222	−2.747	
^{141}Ho$^{\rm m}$	1.251	$(1/2^+) \to 0^+$	0	0.31	6.74	76.03	−5.137	−6.220	
^{145}Tm	1.741	$(11/2^-) \to 0^+$	5	3.06	6.35	62.10	−5.499	−5.520	−5.14
^{146}Tm	0.891	$(1^+) \to 1/2^+\#$	0	0.31	6.79	109.95	−0.810	−0.850	
^{146}Tm$^{\rm m}$	1.201	$(5^-) \to 1/2^+\#$	5	3.06	6.36	87.54	−1.125	−0.976	
^{147}Tm	1.059	$11/2^- \to 0^+$	5	3.06	6.37	98.51	0.573	0.710	0.98
^{147}Tm$^{\rm m}$	1.120	$3/2^+ \to 0^+$	2	1.91	6.71	88.73	−3.444	−3.373	−3.39
^{150}Lu	1.271	$(5^-, 6^-) \to (1/2^+)$	5	3.06	6.42	85.15	−1.201	−1.201	−0.58
^{150}Lu$^{\rm m}$	1.291	$(1^+, 2^+) \to (1/2^+)$	2	0.31	6.85	78.13	−4.398	−4.561	−4.38
^{151}Lu	1.243	$11/2^- \to 0^+$	5	3.06	6.43	86.93	−0.914	−0.916	−0.67
^{151}Lu$^{\rm m}$	1.291	$(3/2^+) \to 0^+$	2	1.62	6.77	79.34	−4.783	−4.593	−4.88
^{155}Ta	1.451	$(11/2^-) \to 0^+$	5	3.07	6.50	77.10	−2.495	−2.463	−4.65
^{156}Ta	1.021	$(2^-) \to 7/2^-\#$	2	1.63	6.82	102.77	−0.828	−0.661	−0.38
^{156}Ta$^{\rm m}$	1.111	$(9^+) \to 7/2^-\#$	5	3.07	6.50	99.04	0.924	1.312	1.66
^{157}Ta	0.941	$1/2^+ \to 0^+$	0	0.32	6.93	110.23	−0.529	−0.301	−0.43
^{159}Re$^{\rm m}$	1.816	$1/2^+ \to (8^+)$	5	3.07	6.56	64.11	−4.666	−4.831	
^{160}Re	1.271	$(2^-) \to 7/2^-\#$	2	1.64	6.87	85.04	−3.164	−3.244	−3.0
^{161}Re	1.201	$1/2^+ \to 0^+$	0	0.32	6.98	88.76	−3.357	−3.325	−3.46
^{161}Re$^{\rm m}$	1.321	$11/2^- \to 0^+$	5	3.08	6.58	86.20	−0.680	−0.771	−0.6
^{164}Ir$^{\rm m}$	1.844	$9^+ \to 7/2^-$	5	3.09	6.63	64.64	−4.137	−4.625	−3.92
^{165}Ir$^{\rm m}$	1.721	$(11/2^-) \to 0^+$	5	3.09	6.65	68.92	−3.430	−3.790	−3.51
^{166}Ir	1.161	$(2^-) \to (7/2^-)$	2	1.66	6.95	95.43	−0.842	−1.356	−1.11
^{166}Ir$^{\rm m}$	1.331	$(9^+) \to (7/2^-)$	5	3.09	6.65	87.63	−0.091	−0.369	−0.21
^{167}Ir	1.071	$1/2^+ \to 0^+$	0	0.32	7.05	102.21	−1.128	−1.002	−1.21
^{167}Ir$^{\rm m}$	1.246	$11/2^- \to 0^+$	5	3.10	6.67	93.25	0.778	0.534	0.69
^{170}Au	1.471	$(2^-) \to (7/2^-)$	2	1.67	7.00	77.49	−3.487	−4.194	
^{170}Au$^{\rm m}$	1.751	$(9^+) \to (7/2^-)$	5	3.11	6.72	69.34	−2.975	−3.602	
^{171}Au	1.448	$(1/2^+) \to 0^+$	0	0.32	7.10	77.61	−4.652	−4.829	−5.02
^{171}Au$^{\rm m}$	1.702	$11/2^- \to 0^+$	5	3.11	6.73	71.20	−2.587	−3.243	−3.03
^{176}Tl	1.261	$(3^-, 4^-, 5^-) \to (7/2^-)$	0	0.32	7.15	91.39	−2.208	−2.269	
^{177}Tl	1.155	$(1/2^+) \to 0^+$	0	0.32	7.16	99.80	−1.178	−0.911	−1.36
^{177}Tl$^{\rm m}$	1.962	$(11/2^-) \to 0^+$	5	3.12	6.82	63.77	−3.459	−4.664	−4.49
^{185}Bi$^{\rm m}$	1.607	$1/2^+ \to 0^+$	0	0.32	7.27	73.52	−4.192	−5.263	−5.44

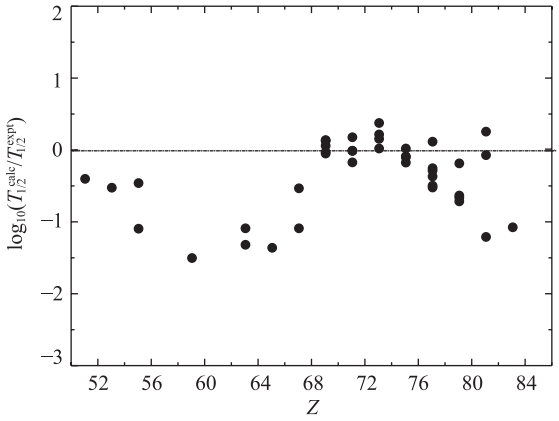

Fig. 2 Decimal logarithm deviations between the experimental data of proton radioactivity half-lives and calculations in this work.

imental data. It may be caused by uncertain angular momentum l which has a significant effect on proton radioactivity. In addition, comparing the present work with the single–folding model, the standard deviation value $\sigma_{\rm sfm}=0.599$, $\sigma_{\rm p}=0.412$ which are from 26 proton decay nuclei in Basu *et al.* and present work, respectively. These results show that the improvement of Coulomb potential is very successful.

In the following, we predicate the proton radioactivity half–lives of 16 nuclei(the proton radioactivity is energetically allowed or observed but not yet quantified in NUBASE2016) in region $53\leqslant Z\leqslant 83$ within two–potential approach with folding potentials. The results are listed in Table 2. In this table, the first seven columns are same as Table 1, the last column is the predicted proton radioactivity half–life shown as $\log_{10}T^{\rm calc}_{1/2}$. The spin and parity are taken from the NUBASE2016[36], the proton radioactivity released energies are taken from the AME2016[37–38]. The predicted proton emitters are in the same region with 41 proton radioactivity nuclei which the value $\sigma=0.614$, thus the predicted proton radioactivity half–lives are within a factor of 4.11. Theoretical predictions[40–43] about the half–life of proton radioactivity have been extensively studied, these results have important reference significance. Therefore, we hope that our predicted can also be useful for future detection in neutron–deficient nuclei around the drip lines.

The Geiger–Nuttall law[44] for proton radioactivity nuclei ^{111,112,113}Cs, ^{170,172}Au, ^{172}Au$^{\rm m}$, ^{144,145,147}Tm, ^{146}Tm$^{\rm m,n}$, and ^{164,165,166,167,169}Ir$^{\rm m}$ are investigated and the linear relationships between $\log_{10}T^{\rm calc}_{1/2}$ and $Q_{\rm p}^{-1/2}$ are plotted in Fig. 3. Different from the α decay and cluster radioactivity where the centrifugal contribution can be reasonably neglected, the proton radioactivity half–life is very sensitive to orbital angular momentum l[45–46]. In addition, the calculated proton radioactivity half–lives of ^{111}Cs, ^{172}Au, ^{172}Au$^{\rm m}$, ^{144}Tm, ^{146}Tm$^{\rm m}$ and ^{169}Ir$^{\rm m}$ are taken from Table 2. In Fig. 3, we can find that the $\log_{10}T^{\rm calc}_{1/2}$ are linearly dependent on $Q_{\rm p}^{-1/2}$ with the angular mo-

Table 2 Same as Table 1, but for predicted radioactivity half–lives of nuclei in region $53\leqslant Z\leqslant 83$, which proton radioactivity are energetically allowed or observed but not yet quantified in NUBASE2016[36], within two–potential approach with folding potentials.

Nucleus	$Q_{\rm p}$/MeV	$j^{\pi}_{\rm p}\to j^{\pi}_{\rm d}$	$l_{\rm min}$	R_1/fm	R_2/fm	R_3/fm	$\log_{10}T^{\rm calc}_{1/2}$
^{108}I	0.601	$1^+\#\to 5/2^+\#$	3	2.21	6.00	127.92	0.602
^{111}Cs	1.811	$3/2^+\#\to 0^+$	2	1.50	6.21	44.56	−12.054
^{117}La	0.821	$(3/2^+)\#\to 0^+\#$	2	1.52	6.27	99.81	−3.054
^{127}Pm	0.911	$5/2^+\#\to 0^+$	2	1.55	6.43	96.34	−3.03
^{137}Tb	0.831	$11/2^-\#\to 0^+$	5	3.12	6.20	117.37	3.071
^{141}Ho	1.181	$(7/2^-)\to 0^+$	3	2.36	6.54	83.09	−3.799
^{144}Tm	1.711	$(10^+)\to 9/2^-\#$	5	3.07	6.33	63.09	−5.302
^{146}Tm$^{\rm n}$	1.131	$(10^+)\to 11/2^-\#$	5	3.06	6.35	92.61	−0.151
^{159}Re	1.591	$1/2^+\#\to 0^+$	0	0.32	6.96	67.03	−7.077
^{165}Ir	1.541	$1/2^+\#\to 0^+$	0	0.32	7.03	71.06	−6.158
^{169}Ir$^{\rm m}$	0.765	$(11/2^-)\to 0^+$	5	3.10	6.69	148.60	8.686
^{169}Au	1.931	$1/2^+\#\to 0^+$	0	0.32	7.09	58.21	−8.496
^{172}Au	0.861	$(2^-)\to 7/2^-\#$	2	1.68	7.01	131.60	4.232
^{172}Au$^{\rm m}$	0.611	$(9^+)\to 13/2^+$	2	1.68	7.01	184.98	10.984
^{185}Bi	1.523	$9/2^-\#\to 0^+$	5	3.15	6.91	82.55	−0.897
^{185}Bi$^{\rm n}$	1.703	$13/2^+\#\to 0^+$	6	3.50	6.79	76.13	−1.080

mentum l remaining the same. With the change of the angular momentum l, the intercept and slope in the figure will be affected and changed in succession. Therefore, the Geiger–Nuttall law also well confirms the above–mentioned statement about the effect of proton radioactivity on angular momentum l. In brief, it indicates that the Geiger–Nuttall law can be used to describe the proton radioactivity and our predictions are reliable.

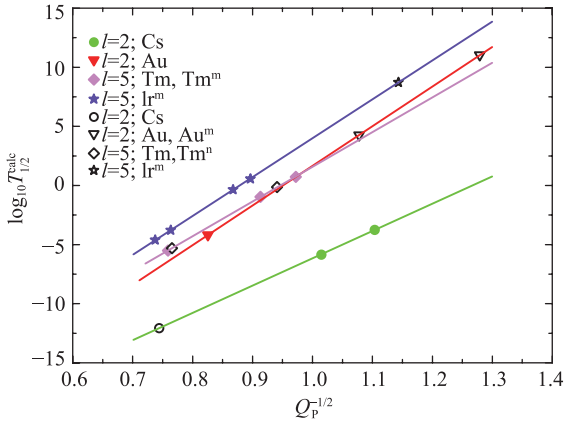

Fig. 3 (color online) The Geiger–Nuttall law for different cases of proton radioactivity between $\log_{10}T_{1/2}^{\rm calc}$ and $Q_{\rm P}^{-1/2}$. The nuclei denoted as solid color and hallow icons are taken from Table 1 and Table 2, respectively.

4 Summary

In summary, we systematically calculate the proton radioactivity half–lives of 41 nuclei from ^{105}Sb to ^{185}Bi^m within the two–potential approach with folding potentials. The calculated results are in good agreement with the experimental data. We also extend our study to predict proton radioactivity half–lives of 16 nuclei(proton radioactivity are energetically allowed or observed but not yet quantified in NUBASE2016) in the same region, and the predicted proton radioactivity half–lives are within a factor of 4.11. In addition, the Geiger–Nuttall law is shown that it can be used to describe the proton radioactivity isotopes with same angular momentum.

References:

[1] JACKSON K P, CARDINAL C U, EVANS H C, *et al.* Phys Lett B, 1970, **33**: 281.
[2] CERNY J, ESTERL J, GOUGH R A, *et al.* Phys Lett B, 1970, **33**: 284.
[3] HOFMANN S, REISDORF W, MÜNZENBERG, *et al.* Z Phys A, 1982, **305**: 111.
[4] KLEPPER O, BATSCH T, HOFMANN S, *et al.* Z Phys A, 1982, **305**: 125.
[5] BUCK B, MERCHANT A C. Phys Rev C, 1992, **45**: 1688.
[6] BLANK B, BORGE M J G. Prog Part Nucl phys, 2008, **60**: 403.
[7] THOENNESSEN M. Nuclear Physics Review, 2016, **33(2)**: 117.
[8] KARNY M, RYKACZEWSKI K P, CRZYWACZ R K, *et al.* Phys Lett B, 2008, **664**: 56.
[9] BASU D N, ROY CHOWDHURY P, SAMANTA C. Phys Rev C, 2005, **72**: 051601(R).
[10] ROY CHOWDHURY P, SAMANTA C, BASU D N. At Data Nucl Data Tables, 2008, **94**: 781.
[11] BHATTACHARYA M, GANGOPADHYAY G. Phys Lett B, 2007, **651**: 263.
[12] BALASUBRAMANIAM M, ARUNACHALAM N. Phys Rev C, 2005, **71**: 014603.
[13] DUARTE S B, TAVARES O A P, GUZMÁN G, *et al.* At Data Nucl Data Tables, 2002, **80**: 235.
[14] DONG J M, ZHANG H F, ROYER G. Phys Rev C, 2009, **79**: 054330.
[15] ZHANG H F, WANG Y J, DONG J M, *et al.* J Phys G: Nucl Part Phys, 2010, **37**: 085107.
[16] ZHANG Hongfei. Nucl Phys Rev, 2016, **33(2)**: 167.
[17] GURVITZ S A, SEMMES P B, NAZAREWICZ W, *et al.* Phys Rev A, 2004, **69**: 042705.
[18] GURVITZ S A, KALBERMANN G. Phys Rev Lett, 1987, **59**: 262.
[19] SUN X D, DENG J G, XIANG D, *et al.* Phys Rev C, 2016, **93**: 034316.
[20] SUN X D, GUO P, LI X H. Phys Rev C, 2016, **94**: 024338.
[21] SUN X D, WU X J, ZHENG B, *et al.* Chin Phys C, 2017, **41**: 014102.
[22] SUN X D, DENG J G, XIANG D, *et al.* Phys Rev C, 2017, **95**: 044303.
[23] SUN X D, DUAN C, DENG J G, *et al.* Phys Rev C, 2017, **95**: 014319.
[24] DENG J G, CHENG J H, ZHENG B, *et al.* Chin Phys C, 2017, **41**: 124109.
[25] DENG J G, ZHAO J G, XIANG D, *et al.* Phys Rev C, 2017, **96**: 024318.
[26] DENG J G, ZHAO J G, CHEN J L, *et al.* Chin Phys C, 2018, **42**: 044102.
[27] BERTSCH G, BORYSOWICZ J, MCMANUS H, *et al.* Nucl Phys A, 1977, **284**: 399.
[28] SATCHLER G R, LOVE W G. Phys Rep, 1979, **55**: 183.
[29] KOBOS A M, BROWN B A, HODGSON P E, *et al.* Nucl Phys A, 1982, **384**: 65.
[30] HAHN B, RAVENHALL D G, HOFSTADTER R. Phys Rev, 1956, **101**: 1131.
[31] GUPTA D, BASU D N. Nucl Phys A, 2005, **748**: 402.
[32] MADHUBRATA BHATTACHARYA, GANGOPADHYAY G. Phys lett B, 2007, **651**: 263.
[33] CHAUDHURI A M, BROWN B A, LINDSAY R, *et al.* Nucl Phys A, 1984, **425**: 205.
[34] BASU D N. J Phys G: Nucl Part Phys, 2004, **30**: B7.
[35] MOREHEAD J J. J Math Phys, 1995, **36**: 5431.
[36] AUDI G, KONDEV F, WANG M, *et al.* Chin Phys C, 2017, **41**: 030001.

[37] HUANG W J, AUDI G, WANG M, *et al*. Chin Phys C, 2017, **41**: 030002.
[38] WANG M, AUDI G, KONDEV F, *et al*. Chin Phys C, 2017, **41**: 030003.
[39] BUDACA R, BUDACA A I. Eur Phys J A, 2017, **53**: 160.
[40] QIAN Y B, REN Z. Eur Phys J A, 2016, **52**: 68.
[41] RAJESWARI N S, BALASUBRAMANIAM M. Eur Phys J A, 2014, **50**: 105.
[42] WANG Y Z, GU J Z. Phys Rev C, 2017, **95**: 014302.
[43] WANG J M, ZHANG H F, LI J Q. J Phys G: Nucl Part Phys, 2014, **41**: 065102.
[44] GEIGER H, NUTTALL J M. Phylos Mag, 1911, **22**: 613.
[45] ZDEB A, WARDA M, POMORSKI K. Phys Rev C, 2013, **87**: 024308.
[46] ZDEB A, WARDA M, PETRACHE C M, POMORSKI K. Eur Phys J A, 2016, **52**: 323.

基于折叠势的两势方法系统研究质子放射性

陈玖龙[1]，程俊皓[1]，邓军刚[1]，李小华[1,2,†]

（1. 南华大学核科学技术学院，湖南 衡阳　421001；
2. 湖南师范大学低维量子结构与调控教育部重点实验室，长沙　410081）

摘要： 基于两势方法系统地研究了质子数 $51 \leqslant Z \leqslant 83$ 质子放射性核素的衰变半衰期。总的质子–子核相互作用势包括：通过单折叠子核密度和 DDM3Y 有效相互作用得到的微观核势，通过单折叠子核电荷密度和质子-质子库仑相互作用得到的真实库仑势以及离心势。同时，预测了同一区域 16 个核的质子放射性半衰期，并且预测的质子放射性半衰期在 4.11 倍的范围内。此外，还研究了质子放射性的 Geiger–Nuttall 定律。结果表明，Geiger–Nuttall 定律可以用来描述角动量相同的同位素的质子放射性。

关键词： 质子放射性；两势方法；折叠势；Geiger–Nuttall 定律

收稿日期： 2018-05-13；　**修改日期：** 2018-06-30

基金项目： 国家自然科学基金资助项目 (11205083, 11505100)；湖南省重点学科 (核科学与技术)，湖南省教育厅重点项目 (15A159)；湖南省自然科学基金资助项目 (2015JJ3103, 2015JJ2121)；南华大学粒子物理与原子核物理创新团队；山东省自然科学基金项目 (ZR2015AQ007)

† **通信作者：** 李小华，E-mail: lixiaohuaphysics@126.com。